Nanometer scale tomographic investigation of fine scale precipitates in a CuFeNi granular system by 3D FIM

(Article begins on next page)

19 April 2024

iris - AperTO

Nanometer Scale Tomographic Investigation of Fine Scale Precipitates in a CuFeNi Granular System by Three-Dimensional Field Ion Microscopy

Sophie Cazottes,[1] François Vurpillot,[1] Abdeslem Fnidiki,[1]* Dany Lemarchand,[1] Marcello Baricco,[2] and Frederic Danoix[1]

[1]Groupe de Physique des Matériaux, Université de Rouen, UMR CNRS 6634, Site Universitaire du Madrillet,BP12, 76801 Saint Etienne du Rouvray cedex, France

[2]Dipartimento di Chimica IFM and NIS/INSTM, Università di Torino, Via P.Giuria 9, 10125 Torino, Italy

Abstract: The microstructure of $Cu_{80}Fe_{10}Ni_{10}$ at. % granular ribbons was investigated by means of three-dimensional field ion microscopy 3D FIM . This ribbon is composed of magnetic precipitates embedded in a nonmagnetic matrix. The magnetic precipitates have a diameter smaller than 5 nm in the as-spun state and are coherent with the matrix. No accurate characterization of such a microstructure has been performed so far. A tomographic characterization of the microstructure of melt spun and annealed $Cu_{80}Fe_{10}Ni_{10}$ ribbon was achieved with 3D FIM at the atomic scale. A precise determination of the size distribution, number density, and distance between the precipitates was carried out. The mean diameter for the precipitates is 4 nm in the as-spun state. After 2 h at 3508C, there is an increase of the size of the precipitates, while after 2 h at 4008C the mean diameter of the precipitates decreases. Those data were used as inputs in models that describe the magnetic and magnetoresistive properties of this alloy.

Key words: 3D field ion microscopy, granular materials, structural characterization, CuFeNi

INTRODUCTION

Relatively high giant magneto resistance GMR values were measured on CuFeNi melt spun ribbons Chen et al., 1994, 1996; Martins et al., 1998; Martins & Missel, 1999; Baricco et al., 2004 . This GMR effect is attributed to the presence of fine scale magnetic precipitates embedded in a nonmagnetic matrix. In granular alloys, the GMR effect is strongly depen-dent on microstructural parameters, such as the precipitate size distribution, the composition of the matrix and of the precipitates, the precipitates number density, and the dis-tance between precipitates and their morphology. Several models have been proposed to correlate the GMR effect and structural parameters Chuang et al., 1985; Zhang & Levy, 1993; Allia et al., 1995; Ferrari et al., 1997 . Zhang and Levy 1993 developed a model for which, in the case of a broad size distribution of the magnetic precipitates, a maximum of the GMR value is obtained for a critical particle diameter. Moreover, the model developed by Ferrari et al. 1997 takes into account the presence of superparamagnetic precipitates to describe the magneto resistance MR data. The size distri-butions of the precipitates as well as the saturation magneti-zation are used to calculate theoretical MR curves that can be compared with the experimental curves. The more pre-cise the inputs are in such fitting procedures, the easier it is to interpret agreements or deviations from the model.

However, the structural parameters strongly depend on the history of each studied ribbon, in particular on the elaboration and subsequent heat treatment conditions. In Martins et al. 1998 , the composition of the ribbon was $Cu_{80}Fe_{10}Ni_{10}$ at. % and the structural parameters of the precipitates were deduced from magnetization curves and Mössbauer spectra. In addition, Mössbauer spectroscopy has made possible a link between structural and magnetic observations Eymery et al., 1983, 2003; Richomme et al., 1996; Fnidiki et al., 1998; Lemoine et al., 1999; Juraszek et al., 2000; Duc et al., 2002 . Those magnetic analyses revealed the presence of fine body-centered cubic A-Fe precipitates with a radius slightly larger than 1 nm. In Martins and Missel 1999 , some spinodally decomposed Fe,Ni - rich zones were observed by high-resolution trans-mission electron microscopy HRTEM in a $Cu_{63}Fe_{18}Ni_{19}$ at. % ribbon. In Baricco et al. 2004 , X-ray diffraction measurements were performed on $Cu_{802x}Fe_{20}Ni_x$ x 5 0, 5, 20 ribbons indicating the presence of A-Fe for $Cu_{80}Fe_{20}$ and $Cu_{75}Fe_{20}Ni_5$ ribbons. Other studies evidenced the pres-ence of fine scale face-centered cubic fcc Fe,Ni -rich precipitates embedded in a fcc Cu-rich matrix Chen et al., 1994; Cazottes et al., 2008 . All those different microstruc-tures can be explained by the fact that the ribbons are in a nonequilibrium state and that their microstructures are highly dependent on the elaboration technique and param-eters. This bibliographical survey leads to the conclusion that each single ribbon should be characterized to get its own microstructural information. Moreover, there is a large discrepancy between the size observed using direct observa-tions, such as by transmission electron microscopy TEM or HRTEM, and the one derived from magnetization curves. These latter are usually underestimated as compared to direct observations when available. Considering the small

size of the precipitates and the fact that in this system the precipitates and the matrix have similar lattice parameters, it is quite difficult to determine precisely the size and size distribution of the particles using conventional TEM observation Cazottes et al., 2008 . Thus, alternative analytical techniques are required for the analysis of such samples.

This article presents a newly developed technique, namely three-dimensional field ion microscopy 3D FIM Jessner et al., 2007; Vurpillot et al., 2007; Semboshi et al., 2009 , for a precise characterization of the size, the morphol-ogy, and the structure of the precipitates in $Cu_{80}Fe_{10}Ni_{10}$ at. % ribbons, in its as-spun and annealed at different temperature conditions.

MATERIALS AND METHODS

Sample Preparation

Master alloys of $Cu_{80}Fe_{10}Ni_{10}$ at. % have been prepared by arc melting of pure elements. Ribbons were obtained by a planar-flow casting process in an inert atmosphere using a Cu-Zr wheel. Typical values for overpressure and peripheral wheel velocity were around 0.4 atm and 18 ms[21], respec-tively. The ribbons were 5 mm wide, 60 Mm thick, and several meters long. Literature reports good GMR proper-ties for such ribbons after annealing at 4008C for 2 h Martins et al., 1998 . To determine the parameters influenc-ing the evolution of the GMR, a structural analysis was made on ribbons in the as-spun condition and annealed at 3508C and at 4008C for the same duration.

FIM samples were prepared in the form of sharp tips with a radius of curvature close to 50 nm. Tips were prepared by electropolishing @10 g Na_2CrO_4 H_2O $_4$ 1 100 mL acetic acid, 8 V, 300 K# and then thinned with a focused ion beam FIB using annular milling at 30 kV Larson et al., 1999 . Tips made out of CuFeNi ribbons are very brittle at the observation temperature usually 20 to 40 K , and the high electric field applied to the tip often causes the failure of the specimen. With hydrogen and a high temperature, the failure probability is lowered and the success rate for the observation is higher. Field ion micrographs were obtained using hydrogen as the imaging gas pressure of 2 3 10^{23} Pa . The hydrogen was also chosen because it reinforces the contrast between the two phases. The tip temperature was 110 K.

Field Ion Microscopy

FIM is based on field ionization Wei et al., 1981; Cerezo et al., 1992; Blavette et al., 1993; Miller et al., 1996; Vau-mousse et al., 2003; Vurpillot et al., 2007 . For that purpose, tips are submitted to a high positive voltage 3–15 kV . The image of the surface of the tip is produced by the field ionization of gas atoms at the tip surface by the projection of the atoms onto a screen. By increasing the potential applied to the tip, individual atoms from the surface are evaporated, so that the sample can be imaged in its depth.

The evaporation sequence is recorded on a digital cam-era. Individual digital micrographs can be extracted from the filmed sequence, which usually contains several minutes of data acquisition and represents the evaporation of several hundred atomic layers. Each micrograph is a snapshot of the sample atomic surface at a certain evaporation depth. As the Fe,Ni -rich phase has a higher evaporation field than the copper matrix, it appears in bright contrast in the darker Cu-rich matrix. Individual micrographs are used to reconstruct the evaporated volume in 3D, using Amirat software, according to the reconstruction procedure de-scribed in Vurpillot et al. 2007 . This tomographic recon-struction has a size of about 100 3 100 3 50 nm^3. The digital definition of the final 3D image is about 500 3 500 3 1000 points voxel size ; 0.2 3 0.2 3 0.05 nm^3 . The lateral dimensions of the reconstructed volume were calibrated using the Drechsler method Vurpillot et al., 2007 , whereas the depth scale was determined by counting the number of evaporated atomic planes. Considering their high evapora-tion field and the high temperature used, the precipitates are subject to the well-known local magnification effect Miller & Hetherington, 1991 , and thus their lateral dimen-sions are overestimated. As mentioned in Vurpillot et al. 2007 , a linear voltage variation was applied to the speci-men in order to reach a constant evaporation rate.

RESULTS

3D FIM snapshots extracted from the evaporation sequence of the $Cu_{80}Fe_{10}Ni_{10}$ as-spun ribbon are presented in Fig-ures 1a and 1b. A large Fe, Ni -rich precipitate is observed on the lower left-hand part of the micrographs. Its size corresponds to the one of large intergranular precipitates observed by energy filtered TEM Cazottes et al., 2008   see Fig. 1c . On Figure 1b, at the interface between this precipi-tate and the Cu-rich matrix, a 111 pole is visible. As the characteristic circles are continuous within the two phases, the crystallographic lattice is continuous between the precip-itate and the Cu-rich phase, indicating that this precipitate is coherent or at least semicoherent with the Cu matrix.

Figure 2 presents the tomographic reconstruction of the as-spun ribbon. Although no intragranular precipitate is visible on two-dimensional 2D micrographs see Fig. 1 , a contrast appears on the tomographic representation indicat-ing the presence of the Fe, Ni -rich precipitates. Revealing hidden contrasts is a major advantage of 3D FIM analysis. A second advantage is to provide a fully 3D reconstruction at the near atomic level, which allows accurate size distribu-tion measurements, distance distribution measurements, and morphology measurements. Figure 3 shows atomic planes that are visible inside the intergranular Fe, Ni precipitate.

The presence of precipitates clearly indicates that, dur-ing quenching, the cooling rate was not high enough to prevent the precipitation of Fe, Ni -rich precipitates and thus produces a single phase solid solution. After exploring the volume in different directions, it is clear that the precip-itates are not interconnected even if their density is very high and if they sometimes are in contact. The precipitates appear roughly spherical and their diameter was measured directly on the volume see Fig. 3 . Note that some artificial deformations of the precipitates are observed at the border of the volume due to incorrect reconstructions far from the tip axis. For these angles, both the projection law and the tip shape assumption hemispherical shape are rather rough approximations. To avoid these artifacts, regions of the border of the volume will be removed for all statistical measurements.
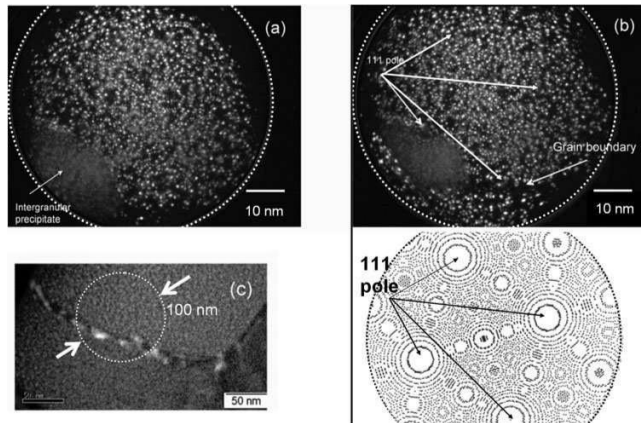

Figure 1. a, b: FIM image of the as-spun $Cu_{80}Fe_{10}Ni_{10}$ under a hydrogen pressure of 2 3 10^{25} Torr. The diameter of the imaging area is approximately 100 nm. A large precipitate appears at a grain boundary in the left-hand bottom part, but no small precipitates are visible inside the grains. Note the presence of 4 111 type crystallographic poles, indexed by FIM simulation bottom of the image . This kind of large precipitate is also observed by EFTEM. **c:** EFTEM iron map, where the bright zones are iron-enriched zones. The circle is an indication of the size of the surface observed by FIM.
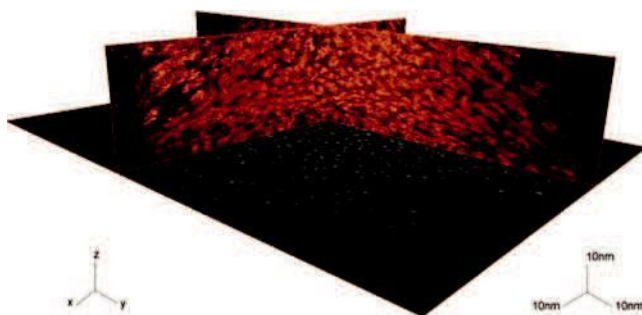

Figure 2. Sections in the reconstructed volume of the $Cu_{80}Fe_{10}Ni_{10}$ as-spun ribbon. The original micrograph lies in the *xy* plane, and the volume is reconstructed along the *z* axis.

An experimental size distribution has been extracted from this reconstructed volume. This distribution was fitted using the lognormal distribution commonly used for mag-netization curves modeling Ferrari et al., 1997 . It gives a mean diameter ^{D} & of 4.1 nm and a dispersion S of 0.30 nm. The diameter is given with a precision of 0.5 nm and the dispersion with a precision of 0.01. The same experimental procedure was used for the 3508C and 4008C annealed sample. Figure 4 shows the precipitation observed in the sample annealed at 3508C for 2 h. The same kind of microstructure as in the as-spun sample was observed, which was also observed by energy filtered transmission
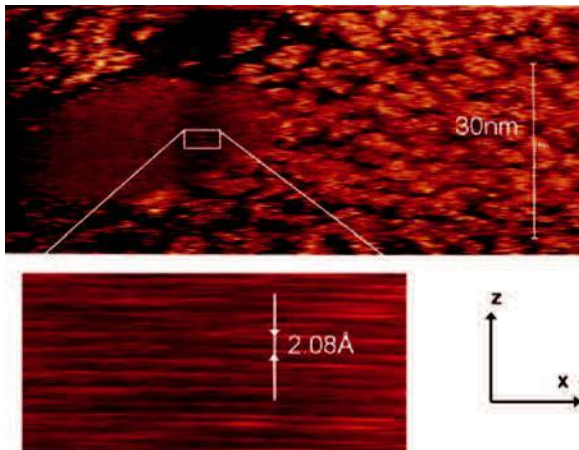
Figure 3. Orthogonal slice in the reconstructed volume of the as-spun ribbon. Only in the 3D reconstruction, the precipitates appear in three dimensions. The white bar represents 30 nm. The image on the bottom is a zoom of the white rectangular area of the slide, exhibiting atomic planes.

electron microscopy EFTEM; Cazottes et al., 2008 . After 2 h at 3508C, there is an increase in the precipitate size, the mean diameter is 4.9 nm, and the dispersion is 0.27 nm. After annealing at 4008C for 2 h, the diameter is closed to the one of the as-spun sample with the mean diameter, $\hat{D}$ & 5 4.2 nm, and a distribution of 0.22 nm. The experi-mental distributions and their lognormal fits are presented in Figure 5. It is worth noting that the determination of the diameter and size distribution can be overestimated with 3D FIM, due to the local magnification effect on the recon-structed volume Miller & Hetherington, 1991 and the use of hydrogen as the imaging gas. This artifact is systematic and generally more pronounced for very small precipitates Blavette et al., 2001 . Since the ionization processes for the image gas and the surface atoms occur at slightly different positions and the trajectories of the ions are influenced by their neighbors, this artifact is less pronounced in FIM than in atom probe Miller & Hetherington, 1991 . According to the local density measured in atom probe on this kind of sample, the average diameter of precipitates is overesti-mated by less than 20% in atom probe measurement. As a result, the accuracy of the precipitate diameters measured in FIM is about 20.5 nm/21 nm, considering the size of precipitates. Note also that single measurements of the diameter are given with a precision of 60.5 nm.
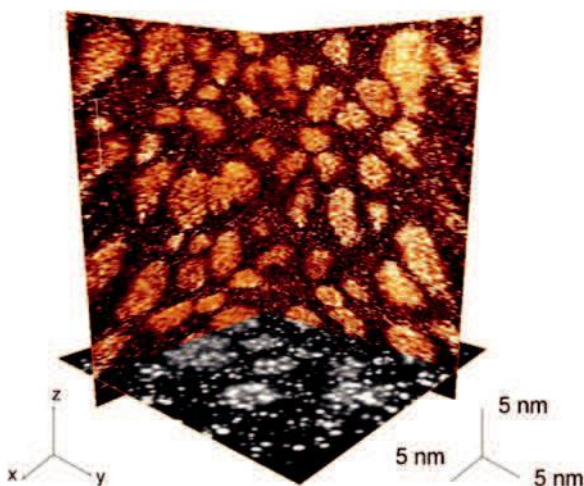

Figure 4. 3D FIM reconstruction of the sample annealed at 3508C for 2 h. The original image is represented in the *xy* plane while the reconstructed images are represented along the *z* axis.
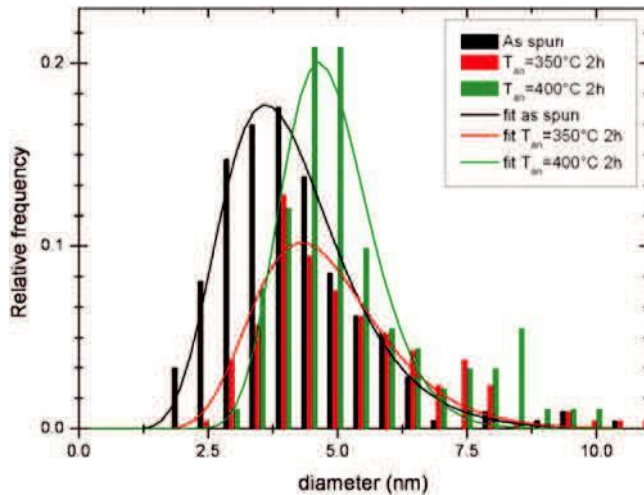
Figure 5. Experimental bars and fitted lines size distributions measured by 3D FIM, for as-spun, 3508C and 4008C heat-treated samples.

DISCUSSION

The major advantage of 3D FIM compared to EFTEM is the possibility of 3D particle counting, without any projection bias. By simply counting the precipitates that are in a given volume, the number density of precipitates can be determined from those analyses. The number density is given with an accuracy of 0.3 3 10^{18} part/cm^3. It is 3.7 3 10^{18} part/cm^3 in the as-spun state; 1.7 3 10^{18} part/cm^3 after annealing at 3508C for 2 h and 5.9 3 10^{18} part/cm^3 for the sample annealed at 4008C for 2 h.

As mentioned above, the distance between the precipi-tates is an important parameter for magnetoresistive mate-rials Chuang et al., 1985; Zhang & Levy, 1993; Allia et al., 1995; Ferrari et al., 1997. Whereas distances measured in 2D as for example in TEM are projected, real distances are measured in 3D. Using those 3D FIM volumes, a precise characterization of the precipitates is possible. The mean distance between precipitates *d* was calculated using the formula *d* 5 1/*N* $^{1/3}$ with *N* the number density of the precipitates. In the as-spun state, the mean distance between the precipitates is 6.4 nm, it reaches 8.4 nm after annealing at 3508C for 2 h and it decreases after annealing at 4008C for 2 h to 5.5 nm. Those *d* parameters are given with an accuracy of 0.3 nm. Using the number density and the mean diameter of the precipitates, the volume fraction is given by f_V 5 P{^*D* &^{3}{*N*/6. It is, respectively, 13.3%, 10.4%, and 22.8% for the as-spun, 3508C, and 4008C annealed samples.

One other advantage of the 3D FIM is the size of the analyzed volume, which is, for this precipitate size, large enough to get a high number of precipitates and therefore good statistical measures, particularly if the size of the precipitates is distributed. As the diameter of the precipi-tates is overestimated, the evolution of their size distribu-tion with temperature is significant but not absolute. Conversely, the number density determined by simply count-ing the number of particles in a given volume is accurate as the reference volume is perfectly known. Also, the distance between particles, which is important for understanding magnetic properties in granular systems, is given with a very good accuracy.

Diameters obtained by 3D FIM, combined with compo-sition determined by atom probe tomography, were used to calculate the mean magnetic moment ^M& of the precipi-tates, using the relation: M 5 x^{Fe}M^{Fe} 1 x^{Ni}M^{Ni} 1 x^{Cu}M^{Cu} with x^i the composition of the precipitate in the element *i* and M^i the theoretical elemental magnetic moment of the element *i*. In our case, M^{Fe} 5 1.34 M$_B$, M^{Ni} 5 0.63 M$_B$, and M^{Cu} 5 0 M$_B$ Mishin et al., 2005. The average magnetic moment per precipitate *M* is calculated using *M* 5 M{*V*{R with V the mean volume of the precipitates and R the atomic density of the precipitates. R is calculated from the lattice parameter determined by X-ray diffraction XRD Cazottes et al., 2008. It is for the as-spun sample, ^M& 5 2238 M$_B$ Cazottes et al., 2009*b*, which is very close to the value derived from magnetization measurements, ^M$_{fit}$& 5 2442 M$_B$ Cazottes, 2008. Those data were used to perform a thorough study on the relation between the microstruc-ture and the magnetic and magnetoresistive properties of such system Cazottes, 2008; Cazottes et al., 2009*a*. Intro-ducing the real magnetic moment of the precipitates in the model revealed that magnetic interactions between the precipitates were not negligible as often considered. An im-proved model was proposed Cazottes, 2008; Cazottes et al., 2009*a*.

CONCLUSIONS

With the aim of providing accurate structural data that would help understanding transport properties in a granu-lar system, 3D FIM measurements were carried out. Using this newly developed technique, structural data such as size distribution, number density, and mean distance between the precipitates could be determined, while techniques such as XRD measurements and energy filtered imaging TEM did not provide convincing results for this kind of material. We have evidenced the presence of fine isostructural and coherent Fe,Ni -rich precipitates inside a Cu-rich phase in $Cu_{80}Fe_{10}Ni_{10}$ at. % melt-spun and annealed ribbons. For the three different heat treatments, the microstructure is composed of two fcc phases: a Cu-rich matrix and small Fe,Ni -rich precipitates located inside the grains. Using 3D FIM, we were able to visualize the Fe,Ni -rich precipitates in three dimensions. In the as-spun state, the mean diam-eter of the precipitates is 4.1 nm. After annealing at 3508C for 2 h, it rises to 4.9 nm. The diameter of the precipitates is decreased after annealing at 4008C for 2 h, down to 4.2 nm.

REFERENCES

Allia, P., Knobel, M., Tiberto, P. & Vinai, F. 1995 . Magnetic properties and giant magnetoresistance of melt-spun granular Cu_{1002x}-Co_x alloys. *Phys Rev B* **52**, 15398–15411.

Baricco, M., Bosco, E., Acconciaioco, G., Rizzi, P. & Coisson, M. 2004 . Rapid solidification of Cu–Fe–Ni alloys. *Mater Sci Eng A* **375**, 1019–1023.

Blavette, D., Bostel, A., Sarrau, J.M., Deconihout, B. &
Menand, A. 1993 . An atom probe for three-dimensional tomography. *Nature* **363**, 432–435.

Blavette, D., Vurpillot, F., Pareige, P. & Menand, A. 2001 . A model accounting for spatial overlaps in 3D atom probe microscopy. *Ultramicroscopy* **89**, 145–153.

Cazottes, S. 2008 . Microstructure à fine échelle d'alliages a propriétés de magnetoresistance géante: relation avec les pro-priétés magnétiques. Cas de rubans $Cu_{80}Fe_xNi_{202x}$ x 5 5,10,15 at% . PhD Thesis, Université de Rouen.

Cazottes, S., Coïsson, M., Fnidiki, A., Lemarchand, D. &Danoix, F. 2009*a* . Influence of magnetic interactions on magnetic and magnetoresistive properties of $Cu_{80}Fe_{10}Ni_{10}$ rib-bons. *J Appl Phys* **105**, 093917–093923.

Cazottes, S., Danoix, F., Fnidiki, A., Lemarchand, D. & Ba-ricco, M. 2009*b* . Influence of structural parameters on magnetoresistive properties of CuFeNi melt spun ribbons.*Ultramicroscopy* **109**, 625–630.

Cazottes, S., Wang, G.Y., Fnidiki, A., Lemarchand, D., Renault, P.O. & Danoix, F. 2008 . Transmission electron microscopy and X-ray diffraction study of microstructural evolution in magnetoresistive Cu–Fe–Ni ribbons. *Philos Mag* **88**, 1345–1356.

Cerezo, A., Hetherington, M.G., Hyde, J.M., Miller, M.K., Smith, G.D.W. & Underkoffler, J.S. 1992 . Visualisation of three-dimensional microstructures. *Surf Sci* **266**, 471–480.

Chen, L.H., Jin, S., Tiefel, T.H., Chang, S.H. & Eibschtuz, M. 1994 . Magnetoresistance in a spinodally decomposed Cu-Ni-Fe alloy consisting of two ferromagnetic phases. *Phys Rev B* **49**, 9194–9197.

Chen, L.H., Jin, S., Tiefel, T.H., Chang, S.H. & Eibschtuz, M.
1996 . Giant magnetoresistance in melt-spun $Cu_{80}Ni_{10}Fe_{10}$ ribbons. *J Appl Phys* **79**, 5599–6001.

Chuang, Y.-Y., Schmid, R. & Austin Chang, Y. 1985 . Calcula-tion of the equilibrium phase diagrams and the spinodally decomposed structures of the Fe-Cu-Ni system. *Acta Met* **33**, 1369–1380.

Duc, N.H., Tuan, N.A., Fnidiki, A., Dorian, C., Teillet, J., Ben Youssef, J. & Le Gall, H. 2002 . Structural, magnetic and Mössbauer studies of Fe-Cu granular films. *J Phys-Condens Mat* **14**, 6657–6666.

Eymery, J.P., Fnidiki, A. & Riviere, J.P. 1983 . CEMS as applied to implantation studies in Fe-Al 40 at-percent. *Nucl Instrum Methods* **209**, 919–942.

Eymery, J.P., Merakeb, N., Goudeau, Ph., Fnidiki, A. & Bouza-bata, B. 2003 . A Mossbauer comparative study in the local environment in metastable 304 stainless steel films depending on the preparation mode. *J Magn Magn Mat* **256**, 227–237.

Ferrari, E.F., Da Silva, F.C.S. & Knobel, M. 1997 . Influence of the distribution of magnetic moments on the magnetization and magnetoresistance in granular alloys. *Phys Rev B* **56**, 6086–6093.

Fnidiki, A., Juraszek, J., Teillet, J., Duc, N.H., Danh, T.M., Kaabouchi, M. & Sella, C. 1998 . Structural and magnetic properties of Ti/Fe multilayers. *J Appl Phys* **84**, 3311–3316.

Jessner, P., Danoix, R., Hannoyer, B., Danoix, F. & Gouné, M. 2007 . Three-dimensional reconstruction of Fe-Cr-nitrides in a Fe-5at%Cr alloy. In *Surface Modification Technology XXI*, Sudarshan, T.S. & Jeandin, M. Eds. , pp. 65–71. Materials Park, OH: ASM International.

Juraszek, J., Fnidiki, A., Teillet, J., Toulemonde, M., Michel, A. & Keune, W. 2000 . Directional effects of heavy-ion irradi-ation in Tb/Fe multilayers. *Phys Rev B* **61**, 12–15.

Larson, D.J., Foord, D.T., Petford-Long, A.K., Liew, H., Blamire, M.G., Cerezo, A. & Smith, G.D.W. 1999 . Field-ion specimen preparation using focused ion-beam milling. *Ultramicroscopy* **79**, 287–293.

Lemoine, C., Fnidiki, A., Lemarchand, D. & Teillet, J. 1999 . Mossbauer and TEM study of Fe-Cr powders elaborated by mechanical alloying. *J Magn Magn Mat* **203**, 184–186.

Martins, C.S. & Missel, F.P. 1999 . Magnetization and giant magnetoresistance in melt-spun and annealed CuFeNi alloys. *J Magn Magn Mater* **205**, 275–282.

Martins, C.S., Rechenberg, H.R. & Missel, F.P. 1998 . Giant magneto resistance in CuFeNi alloys. *J Appl Phys* **83**, 7001–7003.

Miller, M.K., Cerezo, A., Hetherington, M.G. & Smith, G.D.W. 1996 . *Atom Probe Field Ion Microscopy*. Oxford: Clarendon Press.

Miller, M.K. & Hetherington, M.G. 1991 . Local magnifica-tion effects in the atom probe. *Surf Sci* **246**, 442–449.

Mishin, Y., Mehl, M.J. & Papaconstantopoulos, D.A. 2005 . Phase stability in the Fe-Ni system: Investigation by first-principles calculations and atomistic simulations. *Acta Mater* **53**, 4029–4041.

Richomme, F., Fnidiki, A., Teillet, J. & Toulemonde, M. 1996 . Tb/Fe amorphous multilayers: Transformations under ions ir-radiation. *Nucl Instrum Meth B* **107**, 374–380.

Semboshi, S., Al-Kassab, T., Gemma, R. & Kircheim, R. 2009 . Microstructural evolution of Cu-1 at% Ti alloy aged in a hydrogen atmosphere and its relation with the electrical con-ductivity. *Ultramicroscopy* **109**, 593–598.

Vaumousse, D., Cerezo, A. & Warren, P.J. 2003 . A procedure for quantification of precipitate microstructures from three-dimensional atom probe data. *Ultramicroscopy* **95**, 215–221.

Vurpillot, F., Gilbert, M. & Deconihout, B. 2007 . Towards the three-dimensional field ion microscope. *Surf Interface Anal* **39**, 273–277.

Wei, C-Y., Currentland, M.I. & Seidman, D.N. 1981 . Direct observation of the primary state of damage of ion-irradiated tungsten I. Three-dimensional spatial distribution of vacancies.
Philos Mag **44**, 459–491.

Zhang, S. & Levy, P.M. 1993 . Conductivity and magnetoresis-tance in magnetic granular films. *J Appl Phys* **73**, 5315–5319.